JOURNAL OF CATALYSIS 125, 427–444 (1990)

Acid Strength of Silica–Alumina and Silica Studied by Microcalorimetric Measurements of Pyridine Adsorption

NELSON CARDONA-MARTÍNEZ[1] AND J. A. DUMESIC[2]

Department of Chemical Engineering, University of Wisconsin, Madison, Wisconsin 53706

Received February 26, 1990; revised May 9, 1990

Microcalorimetric measurements of the differential heat of pyridine adsorption at 473 K were used to probe the distribution of acid strength on silica and silica-supported alumina catalysts. Depositing alumina on silica increased the acid strength of the catalyst. The acid strength distribution curves for the Al_2O_3/SiO_2 sample showed three regions of constant heat of adsorption while silica had an energetically homogeneous surface. The Al_2O_3/SiO_2 catalyst was found to have both Brønsted and Lewis acidity. Incremental adsorption of pyridine on Al_2O_3/SiO_2 indicated that the initial region of constant heat corresponds to strong Lewis acidity while the intermediate region seemed to be Brønsted sites or a combination of weaker Lewis sites and Brønsted sites. The final region observed at higher extents of adsorption showed only H-bonded pyridine which corresponds to adsorption on silica. Estimates of the entropies of adsorption were determined, providing information about the mobility of the adsorbed basic molecules. Surface diffusion over the silica support provides an important pathway for the equilibration of pyridine between acid sites on the Al_2O_3/SiO_2 sample.

INTRODUCTION

The use of metal oxides as catalysts has important significance for organic synthesis and for the chemical industry. Catalytic cracking, isomerization of hydrocarbons, alkylation of paraffins and aromatics with olefins, polymerization of olefins, and partial oxidation of hydrocarbons are among the reactions carried over metal oxide catalysts (*1, 2*). Hence, there is a significant motivation to gain a better understanding of the surface properties of metal oxides, since it is desired to control these properties to tailor and improve catalysts for existing processes and to design improved catalysts for new catalytic processes such as for the production of specialty chemicals.

The catalytic properties of metal oxide surfaces are typically described in terms of acid–base concepts. Some reactions require acid sites while others occur on basic sites, and on other occasions the same reaction over an acid or a base gives different products (*3*). Those oxides used as industrial catalysts are often multicomponent materials which may possess both acid and base sites (*4*). Catalysts having suitable acid–base pair sites sometimes show pronounced activity and selectivity (*3*), and reactions such as partial oxidation of hydrocarbons (*5*) and dehydrogenation of alcohols (*6, 7*) have been observed to require both types of sites on the surface.

It has been found that the acid–base properties of mixed metal oxides can be varied by choosing different metal oxide constituents at different concentrations and by changing the treatment of the sample (*4*). Thus, it appears that by properly choosing the aforementioned variables, mixed oxides could be used to develop new catalysts with desired acid–base properties. To understand the mechanism of their catalytic action and to predict their catalytic activity and selectivity, quantitative information on their acid–base properties is

[1] Present address: University of Puerto Rico, Chemical Engineering Department, P.O. Box 5000, Mayagüez, Puerto Rico 00709-5000.

[2] To whom correspondence should be addressed.

0021-9517/90 $3.00

needed. The present paper provides part of the foundation for such acid–base characterization studies.

Acid sites may exist in different configurations, and this typically leads to a distribution of strengths. This is in addition to the more general distinction between Lewis and Brønsted acid sites. Among the adsorption sites for a particular reaction there may be a certain number of sites with adequate strength that possess the ability to activate the adsorbed molecule and to form a reactive intermediate. Such sites would be denoted as active sites (*6*). At the same time there may be acid or base sites which are either too weak to activate the reactants or are too strong, causing excessive fragmentation of the reactant or surface reactions that may lead to strongly held species which block and deactivate these sites. Therefore, the determination of the acid–base site strength distributions is of fundamental importance in understanding the catalytic properties of metal oxides.

In general, an acidic catalyst can be characterized for the interaction with an adsorbed species if the number of adsorption sites, their strength, and the nature of the interaction, as well as the chemical nature of the adsorbed species, are determined. Many techniques have been used for this purpose with various degrees of success. Hammett titrations with organic indicators (e.g., *1, 4*) and more recently gravimetric adsorption measurements combined with a spectroscopic technique (e.g., *8–13*) have been widely used to measure the acidic properties of mixed oxides. A successful quantitative method should meet the following list of requirements (*14*):

1. the interaction between the probe molecules and the Lewis or Brønsted acid and base sites should be reliably identified and differentiated;
2. the strength of the individual sites should be determined numerically on a defined scale; and
3. the concentration of each type of surface site should be independently determinable.

These requirements can be met by the combination of a spectroscopic method, in particular IR spectroscopy of adsorbed molecules, and a technique capable of measuring a fundamental thermodynamic quantity characterizing the interaction of a probe molecule with the surface sites, such as the differential heat of adsorption. A reliable and accurate way of determining differential heats of adsorption is microcalorimetry.

The present study uses microcalorimetric measurements and IR spectroscopy of adsorbed pyridine to characterize the acid properties of silica and alumina supported on silica. In a subsequent publication we will extend this study and present results for a series of dilute binary oxides with a wide range of electronegativities.

EXPERIMENTAL

The experimental program used in this study was designed to characterize the acid properties of the metal oxides. Microcalorimetric measurements of the heat of adsorption of pyridine were used to determine both the acid site numbers and strengths. Infrared spectroscopy of adsorbed pyridine was employed to determine what types of acid sites are present for given ranges of differential heats.

Microcalorimetry Apparatus

A schematic representation of the microcalorimetry system is shown in Fig. 1. It consists of a Setaram C80 heatflow microcalorimeter of the Calvet type with a sensitivity of 0.25 mW, connected to a stainless-steel, calibrated, volumetric system. The calorimeter is placed on a heavy-duty jack that permits the calorimeter to be moved during pretreatment of the sample under study such that the sample is not exposed to air. Gaseous pressures are measured by means of either an MKS Baratron Model 598 capacitance manometer for pressures

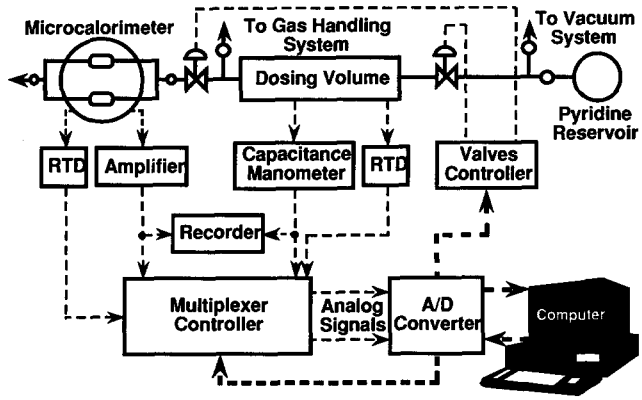

FIG. 1. Schematic of microcalorimetric apparatus.

between 1×10^{-5} and 10 Torr (1 Torr = 133.3 Pa) or a Texas Instruments (TI) precision pressure gauge for pressures between 10 and 1000 Torr. The entire calorimetric system is thermally insulated. The temperature of the volumetric system is kept constant at 318 K using a PID temperature controller. Another temperature controller is used to preheat the gas entering the cells to the calorimeter temperature. This is done to minimize heat effects caused by the heating of the gas that cannot be completely compensated by the reference cell in the calorimeter. The temperatures of the cells and dosing volume are measured using a pair of precision platinum resistance temperature devices (RTD). The dosing volume is attached to a diffusion-pumped glass vacuum system with an ultimate dynamic pressure of 4×10^{-7} Torr and to a gas handling and purification system.

The following quantities are monitored continuously and fed to an Apple IIe computer for subsequent data processing: calorimeter temperature, dosing volume temperature, system pressure, calorimetric signal, and time since dosing. The processing of these data provides a complete characterization of the adsorption process. Calorimetric peak areas and volumetric isotherms give the total heat and total adsorption, respectively, as a function of pressure. Integral heats, Q, as a function of coverage, provide the total acidity of the system. The integral heats accumulated for the successive increments are fitted analytically to an appropriate model. The differential heats, q, are then obtained by differentiation of the integral function with respect to the amount adsorbed, n. Another differentiation with respect to coverage provides the acid strength distribution function $f(q) = -(dn/dq)$. Both of these representations (i.e., differential heats of adsorption as a function of coverage or $f(q)$ as a function of the differential heat of adsorption) provide a description of the acid strength distribution over the surface of the catalyst.

Estimates of the entropy of adsorption can be determined by combination of the adsorption isotherms and the differential heats. Comparison of the experimental and theoretical values by means of statistical thermodynamics allows the degree of mobility of the adsorbed molecules to be probed.

Finally, a study of the thermokinetics of the heat evolution provides additional insight into the adsorption mechanisms. The following thermokinetic parameters can be defined: t_m, $t_{1/2}$, and t_0, which are the times necessary to reach the maximum signal, to decay to one-half of the maximum signal, and to reach the original baseline (*15*). If the amount of heat released in successive doses is of the same order of magnitude,

these parameters provide a semiquantitative description of the kinetics of the adsorption processes taking place on the surface. It has been shown that interpretation of the shapes of individual thermograms facilitates the identification of simultaneous processes with different kinetics as well as the variation of the kinetics with coverage (*16–21*). This technique enables differentiation between strong and weak adsorption (or acidity).

Experimental Procedure

From 0.5 to 1 g of catalyst was placed in the sample cell and degassed for about 2 h at 473 K to reduce the amount of adsorbed molecular water. Following evacuation, oxidation treatments were carried out by passing oxygen through the calorimetric cells at temperatures up to 723 K. The oxygen was purified by passage through a molecular sieve trap at 195 K. The purified treatment gas was passed over the sample at a rate of between 80 and 100 $cm^3\ min^{-1}$. The sample was then heated to the treatment temperature of 723 K in flowing gas. After 4 h of sample activation, the sample was cooled under dynamic vacuum to 473 K. The calorimeter was lifted by the jack to enclose the cells, and the sample was evacuated overnight to allow the system to reach thermal equilibrium at the temperature desired for study. Helium or argon was subsequently used to determine the dead volume of the cells.

The pyridine used in these studies was dried by storage over an activated molecular sieve (3A) and purified with the freeze–pump–thaw technique before each run. The basic molecule was kept in a constant temperature bath to produce a constant vapor pressure of about 4.8 Torr. A known amount of the base was then placed in the calibrated dosing volume. When the pressure in the dosing volume was stable, the probe molecule was dosed into the calorimeter cells, one cell containing the sample, the other serving as a reference. The heat released upon dosing the base was detected by the calorimeter. The signal from the calorimeter was sent to an amplifier and from there to a strip-chart recorder and to a Nelson Analytical Model 761 analog-to-digital interface. The signals from the calorimeter RTD and amplifier, as well as the pressure and dosing volume temperature, were fed to the Apple IIe computer which was programmed to integrate the area under the thermogram, calculate the amount of pyridine adsorbed during the dose, and determine the differential heat of adsorption per mole of adsorbed pyridine as $\Delta Q/\Delta n$. When equilibrium conditions were attained once again, i.e., constant pressure and no deviations from the calorimetric base line, the cells were isolated and the dosing volume was evacuated to decrease the amount of air admitted to the system through small leaks. The above procedure was followed repeatedly. Data were collected until the differential heat of adsorption was in the region of H-bonding on silica. A typical adsorption isotherm was built sequentially from approximately 25 to 40 consecutive doses.

Infrared Spectroscopy of Adsorbed Pyridine

Infrared spectroscopy of adsorbed pyridine was used to determine the types of acid sites present on the silica–alumina samples at different extents of surface coverage. Using the calorimetric measurements discussed in the previous section, the ranges of coverage where the different adsorption processes take place were determined, and IR spectra of adsorbed pyridine were collected at selected points of the adsorption isotherm in those particular ranges. The spectral region from 1400 to 1650 cm^{-1} is particularly important since this range contains IR absorption frequencies expected for coordinated pyridine, pyridinium ion, and hydrogen-bonded pyridine (HPY). Infrared spectroscopy for increasing extents of pyridine adsorption complements the microcalorimetric measurements by indicating the types of sites

present with a given differential heat or given acid strength. The apparatus and procedure used are described below.

Infrared Spectroscopy Apparatus

All infrared spectra were taken at room temperature with a Nicolet 7199 C Fourier transfer infrared spectrometer. The machine parameters used were the same used by Connell (*11*).

All spectra were taken with the samples in a cell consisting of a Pyrex portion where the sample was activated and pyridine was adsorbed and a section with CaF_2 windows where the spectra were collected. The latter section and inlet to the cell were kept at 353 to 373 K during dosing to minimize adsorption of pyridine on the walls. The Pyrex portion has a compartment where an additional amount of sample was placed to decrease the experimental error in determining the amount adsorbed. A standard glass volumetric system with a Texas Instruments precision pressure gauge was used to determine volumetrically the amounts adsorbed. The pyridine was purified in the same manner as described above.

Experimental Procedure

In a typical experiment about 0.4 g of sample was placed in the lower compartment and about 30 mg of sample was pressed into a 1-cm disk. The disk was placed in the sample holder and then pretreated in the same manner as for the microcalorimetry experiments.

After determination of the cell dead volume, the sample was cooled to room temperature and an initial spectrum of the clean sample was taken. This spectrum was subtracted from the subsequent pyridine spectra with baseline correction to show only the pyridine bands. A background spectrum through the CaF_2 windows was collected before each individual spectrum was taken.

The sample was then heated to the adsorption temperature, 473 K. When a constant temperature was obtained, a known amount of pyridine was placed in the dosing volume. When the pressure in the dosing volume was stable, the probe molecule was dosed into the IR cell and the pyridine pressure monitored with the TI gauge. The equilibrium pressure after the first dose was generally lower than the sensitivity of the TI pressure gauge. The sample was subsequently cooled to room temperature, and background and adsorbed pyridine spectra were collected.

The procedure for the second and subsequent doses was necessarily different. After the second dose the equilibrium pressure was measurable and, since the sample had to be cooled to room temperature before the spectra were collected, this gas phase pyridine had to be removed. Therefore, the sample was cooled to 418 K and evacuated for 2 min with a diffusion pump prior to cooling under vacuum to room temperature.

Finally, when hydrogen-bonded pyridine was detected on the surface, the sample was evacuated at 673 K for 1 h and an additional spectrum was collected.

The procedure for the identification of the acid types present is straightforward and has been described for samples equilibrated with a high pyridine pressure and subsequently evacuated at increasing temperatures (*11, 22, 23*). With pyridine in the gas phase (>0.05 Torr), there will be a significant amount of hydrogen-bonded pyridine on the surface. This can be detected by a strong 19b absorption at 1445 cm^{-1} coupled with an 8a band having a weaker peak at 1595 cm^{-1}. Both the 19a and 8b absorptions can be observed, but they are much weaker. If Lewis acid sites are present, a 19b band will appear at 1450 cm^{-1} and a distinct 8a band will appear at a frequency higher than 1600 cm^{-1}. If Brønsted acid sites are present on the surface, a weak 19b band will appear at 1540 cm^{-1}. This will be present in conjunction with an 8a band at 1640 cm^{-1}. In addition, the 19b band at 1490 cm^{-1}, which overlaps for both Lewis and Brønsted sites, is much stronger when

Brønsted sites are present relative to the Lewis acid peak at 1450 cm^{-1}.

For the experimental procedure outlined above, the order of site filling is expected to start with adsorption on Lewis sites, continue with adsorption on Brønsted sites, and end with hydrogen-bonded pyridine.

Sample Preparation

Samples were prepared by incipient wetness impregnation utilizing 1 ml of solution per gram of SiO_2. The silica (Cab-O-Sil grade S-17) was X-ray amorphous (*24*) with a measured BET surface area of 400 $m^2 g^{-1}$. It contained less than 38 ppm total metallic impurities (*24*) and was used without further purification. The small quantities of alumina added did not change the surface area of the catalysts. The Al_2O_3/SiO_2 sample was prepared using aluminum nitrate (99.999%, Aldrich Chemicals) in aqueous solution, followed by drying in air at 390 K for 24 h and calcination in air for 4 h at 723 K.

The aluminum loading was 1.4×10^{17} atoms of Al per square meter of catalyst surface area. This loading corresponds to 0.25 wt% Al and 1.8% of the silicon atoms on the surface. The Al_2O_3/SiO_2 sample was chemically analyzed by Galbraith Laboratories.

RESULTS/DISCUSSION

Pyridine Adsorption on Silica

Silica is a highly electronegative oxide with strong metal-to-oxygen bonds. The surface of silica reacts with water to form neutral hydroxide groups, and strong acidity is not observed experimentally. The integral heat of pyridine adsorption on silica at 473 K as a function of surface coverage for three different runs is shown in Fig. 2. The integral heat of adsorption appears to be linear in the range of coverage studied. Fitting the data to a straight line gives a differential heat of 95 kJ mol^{-1}. Such a heat is considerably higher than the heat of condensation of pyridine, 35.1 kJ mol^{-1} (*25*),

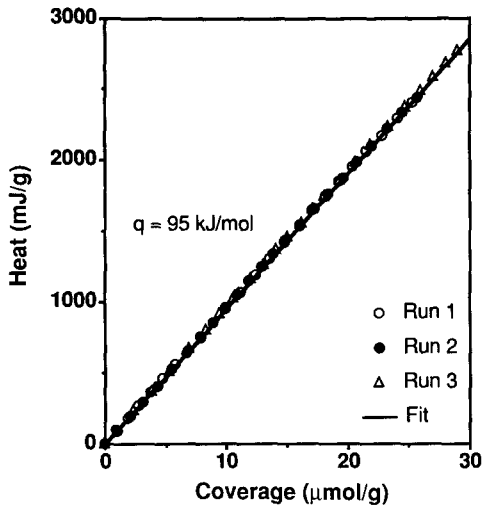

FIG. 2. Integral heat of pyridine adsorbed on three silica samples at 473 K after oxidation at 723 K.

and corresponds to strong hydrogen bonding. This heat compares favorably with the initial differential heat of adsorption of 94 kJ mol^{-1} reported by Kiselev and coworkers (*26*) for the adsorption of pyridine on a macroporous silica–aerosilogel after evacuation at 473 K. The fitted differential heat of adsorption, as well as the average differential heat calculated as $(\Delta Q/\Delta n)_i$ for individual doses, is shown in Fig. 3. The average differential heats for the individual doses show a small negative slope, indicating that the differential heat of pyridine adsorption on silica slowly decreases with increasing coverage. Fitting the integral heat data to a quadratic model, which corresponds to a linear variation of the differential heat of adsorption with coverage, yields an initial differential heat about 1.5 kJ mol^{-1} higher than the value found for the linear model and a negative slope of about -0.1 (kJ mol^{-1}) (μmol g^{-1})$^{-1}$. A summary of these results is presented in Table 1. The change of the differential heat with coverage is small (only 3 kJ mol^{-1} after adsorption of 30 μmol g^{-1} of pyridine), making the average constant differential heat calculated from the linear model adequate for the

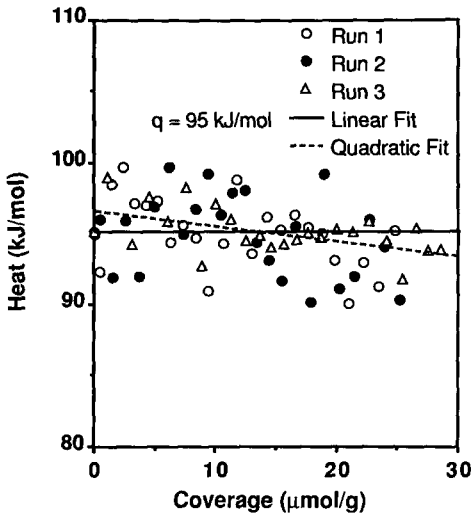

FIG. 3. Average differential heat, $\{\Delta Q/\Delta n\}_i$, of pyridine adsorbed on three silica samples at 473 K after oxidation at 723 K and differential heats of adsorption determined from fitting of integral heat (—, linear model; ----, quadratic model).

range of coverages studied. This is the approach used throughout this work.

The corresponding pyridine adsorption isotherms on silica at 473 K for the three runs are presented in Fig. 4. Note that the adsorption is pressure dependent for the entire range of coverage studied and that the slope at the highest measured coverage is still high, indicating that an appreciable amount of pyridine could still be adsorbed. The adsorption results can be adequately fitted with a Langmuir isotherm as can be seen in Fig. 4. This calculation yields an estimate of the pyridine adsorption equilibrium constant (K), entropy (ΔS_{ads}), and monolayer coverage (n_m). In short, the adsorption of pyridine on silica at 473 K can be described (for the extents of coverage determined) by the following parameters:

$$K = 6.192 \times 10^{-4} \pm 8 \times 10^{-5}\ \text{Pa}^{-1}$$
$$n_m = 140.0 \pm 18.8\ \mu\text{mol g}^{-1}$$
$$q = 95.3 \pm 0.2\ \text{kJ mol}^{-1}$$
$$\Delta S_{ads} = -166.8 \pm 2.6\ \text{J mol}^{-1}\ \text{K}^{-1}.$$

The monolayer coverage determined represents about 56% of the pyridine saturation coverage at 423 K and 650 Pa determined gravimetrically (*27*).

The gas phase absolute entropy of pyridine at 473 K is 328 J mol^{-1} K^{-1} (*25*). Using partition functions along with structural (*28*) and vibrational (*23*) data for pyridine, we can estimate the translational (S_t), rotational (S_r), and vibrational (S_v) contributions to the gas phase entropy. These calculations (see Ref. *29*) give

$$S_t = 173\ \text{J mol}^{-1}\ \text{K}^{-1}$$
$$S_r = 107\ \text{J mol}^{-1}\ \text{K}^{-1}$$
$$S_v = 53\ \text{J mol}^{-1}\ \text{K}^{-1}$$
$$S_{gas} = 333\ \text{J mol}^{-1}\ \text{K}^{-1}$$

TABLE 1

Summary of Regression of the Integral Heat of Adsorption of Pyridine on Silica at 473 K as a Function of Surface Coverage

Model	Variable	Coefficient	Standard error
Linear	Constant	5.814	1.495
	n	95.276	0.096
Quadratic	Constant	−0.701	1.829
	n	96.745	0.304
	n^2	−0.054	0.011

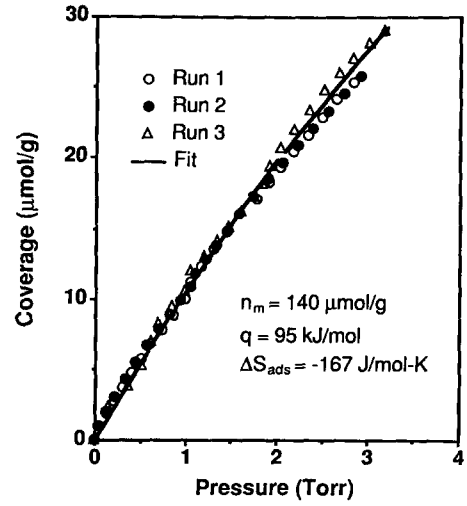

FIG. 4. Isotherms of pyridine adsorption on three silica samples at 473 K after oxidation at 723 K.

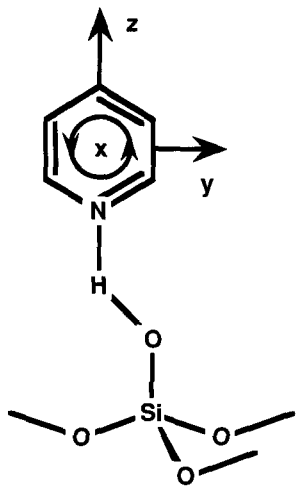

FIG. 5. Graphical representation of a pyridine molecule adsorbed on silica.

The estimated entropy change of adsorption corresponds to a loss of about 50% of the pyridine gas phase entropy. If adsorbed pyridine can be depicted graphically as in Fig. 5, it is reasonable to consider that the molecule should lose some rotational entropy around the x and y axes and to assume that the entropy change along the z axis is small. Also, one degree of translational freedom on the surface must be lost (along the z axis), and we can assume that the change for the vibrational contribution is small. We thereby reach the relation that the entropy of adsorbed pyridine, S^*_{pyr}, is given by

$$S^*_{pyr} = S_v + S_r(z) + S^*_r(x, y) + S^*_t(x, y).$$

Since the value of S^*_{pyr} is 166.2 J mol^{-1} K^{-1}, we find that

$$S^*_r(x, y) + S^*_t(x, y) = 78 \text{ J mol}^{-1} \text{ K}^{-1}.$$

We now assume that the frustrated rotational and translational modes in $S^*_r(x, y) + S^*_t(x, y)$ can be treated as vibrational degrees of freedom. This allows an estimate to be made of an activation energy (E_a) for frustrated translation and rotation by transforming this entropy into a product of terms corresponding to two translational vibrations (υ_t) and two rotational vibrations (υ_r)

$$\exp\left\{\frac{S^*_r(x, y) + S^*_t(x, y)}{R}\right\} = \left\{1 - \exp\left(-\frac{h\upsilon_t}{kT}\right)\right\}^{-2} \left\{1 - \exp\left(-1\frac{h\upsilon_r}{kT}\right)\right\}^{-2}. \quad (1)$$

The translational and rotational frequencies are given approximately by

$$\upsilon_i = \sqrt{\frac{E_a}{2 \text{ MW } a_i^2}}, \quad (2)$$

where MW is the molecular weight of the base and a_i is a characteristic distance for the vibration: the distance between —OH groups for translation and half the circumference of the arcs formed by rotating the molecule around the x or y axes for rotation. Using a_t = 0.309 nm (*30*) and a_r = 0.441 nm in Eqs. (1) and (2), one calculates

$$S^*_r = 42 \text{ J mol}^{-1} \text{ K}^{-1}$$

$$S^*_t = 36 \text{ J mol}^{-1} \text{ K}^{-1}$$

$$E_a = 20.8 \pm 3.4 \text{ kJ mol}^{-1}.$$

The above result suggests that the pyridine retains about 20% of its translational freedom and 60% of its rotational freedom along the x and y axes. Thus, pyridine adsorbed on silica at 473 K is still quite mobile. This result is consistent with a ^{13}C NMR spectroscopy study which indicated that even at 301 K pyridine adsorbed on silica is in a state of rapid motion (*31*). The estimated activation energy for surface diffusion corresponds to 20% of the differential heat of pyridine adsorption on silica which is within the range of values given by Somorjai for surface diffusion on various surfaces (*32*).

If we treat surface diffusion by a random walk analysis, the preexponential factor for diffusion can be shown to be (*32*)

$$A_{\text{diff}} = \frac{\nu d^2 b}{3} N_s^{3/2}, \quad (3)$$

where ν is the surface vibration frequency, b is the molecular diameter of the diffusing species, d is the nearest-neighbor distance, and N_s is the density of active sites. Assuming $\nu = 10^{13}$ s^{-1}, $d = 3.2 \times 10^{-10}$ m, $b = 4.9 \times 10^{-10}$ m, and $N_s = 2 \times 10^{17}$ sites m^{-2}, the preexponential factor is estimated to be 1.5×10^{10} s^{-1}. Using the activation energy estimated earlier, the rate of surface diffusion for a surface pyridine molecule is calculated to be 7.6×10^7 jumps per second, which is more than 2.5×10^5 times higher than the rate of desorption, calculated for the determined heat of adsorption with a frequency factor of 10^{13} s^{-1}. Hence, silica should facilitate the equilibration of pyridine among sites on the surface via surface diffusion.

We can estimate the maximum differential heat that can be measured calorimetrically at 473 K with equilibration among the sites using an expression for the rate constant that corresponds to a quasi-desorption, where the molecule "desorbs" from a strong site to the weaker sites on the support surface. In this case, the appropriate rate constant is given by

$$k_s = \upsilon \exp\left\{\frac{-\Delta q - E_a}{RT}\right\}, \quad (4)$$

where $\Delta q = q - q_s$ is the difference in heat between a strong site and a site on the support, and E_a is the activation energy for surface diffusion. Assuming that 10 desorptions per molecule in an hour is a state approaching equilibrium during the calorimetric experiment, we estimate that the maximum value of $\Delta q + E_a$ possible for equilibrium to be attained is 140 kJ mol^{-1}. If $q_s = 95.3$ kJ mol^{-1} and $E_a = 20.8$ kJ mol^{-1}, then $q = 215$ kJ mol^{-1} at 473 K. This value is much higher than if we require that the molecule must desorb to the gas phase to attain equilibrium. In the latter case, the strongest site that can be studied in an equilibrium fashion is 140 kJ mol^{-1} (i.e., $q_s = E_a = 0$).

In summary, it has been shown above that at high temperatures molecules that are adsorbed on weaker sites may migrate to stronger sites via surface diffusion over the silica support. Hence, as long as the adsorption is done at high temperature and with small sequential doses, the surface will be covered in an ordered manner starting with the strongest sites and ending with the weakest. At 473 K, the strongest site that can be titrated in this manner is estimated to be about 215 kJ mol^{-1}.

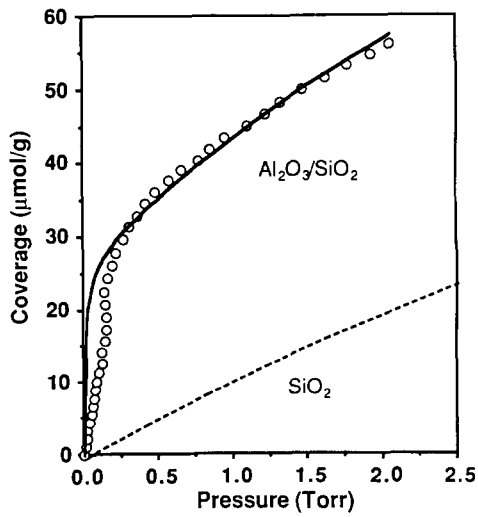

FIG. 6. Isotherms of pyridine adsorption on Al_2O_3/SiO_2 and SiO_2 at 473 K after oxidation at 723 K and fitted isotherm using Langmuir model (O, experimental results; —, Al_2O_3/SiO_2 fit, ---, SiO_2 fit).

Pyridine Adsorption on Aluminum Supported on Silica

Microcalorimetric results. In silica, the silicon cations have a coordination of 4 and the oxygen anions have a coordination of 2. The coordination of 2 for oxygen favors a low coordination for a dopant cation on silica, leading to enhanced acidity. This is observed experimentally as illustrated by the isotherms of pyridine adsorption at 473 K on Al_2O_3/SiO_2 and SiO_2 shown in Fig. 6. Doping SiO_2 with aluminum oxide increases the acidity of the catalyst consider-

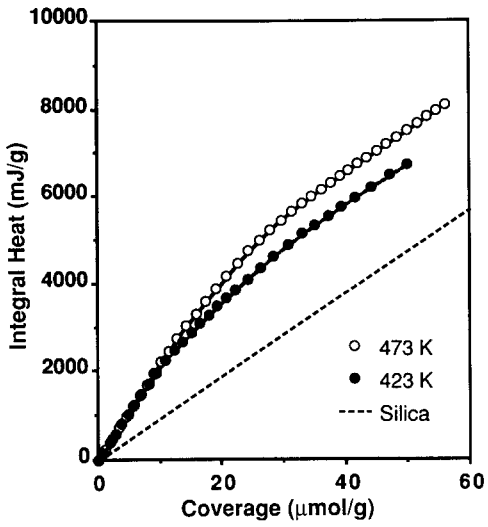

FIG. 7. Integral heat of adsorption for pyridine adsorbed on Al_2O_3/SiO_2 at 423 K and 473 K and on SiO_2 at 473 K after oxidation at 723 K (○, 473 K; ●, 423 K; ---, SiO_2 fit).

ably compared to the acidity on silica. Note that the adsorption is nearly pressure independent at low coverages, suggesting the presence of strong acid sites on Al_2O_3/SiO_2.

Recently, there have been various studies of the effect of the adsorption temperature on the acidic properties of metal oxide catalysts (*33–44*). From these studies it can be concluded that, for samples that possess strong acid sites, using a high adsorption temperature yields a better description of the thermodynamic acid strength distribution. Since adsorption of pyridine on Al_2O_3/SiO_2 leads to high heats of adsorption, we studied the adsorption at 423 and 473 K to test the effect of temperature on the calorimetric data. The integral heat of pyridine adsorption as a function of surface coverage on Al_2O_3/SiO_2 at 423 and 473 K, compared to the fitted integral heat of adsorption over silica at 473 K, is shown in Fig. 7. In contrast to the results for silica, the integral heat plots for Al_2O_3/SiO_2 show significant curvature, indicating that the differential heat of adsorption is not constant on these samples. The integral heat for adsorption at 473 K is higher than that for adsorption at 423 K, the difference increasing as the surface coverage increases. This indicates that the differential heat on the sample where pyridine was adsorbed at 423 K is lower and decreases faster with coverage than that on the sample at 473 K. The difference in behavior is seen more clearly on the corresponding plots for the average differential heat of adsorption as depicted in Fig. 8.

Note the following main features of the curves:

1. an initial region of high, nearly constant heat exists, probably representing adsorption on the strongest sites;
2. a region of gradually declining heats follows, representing adsorption on intermediate acid sites or on a combination of sites; and
3. a region of low differential heats of adsorption (near 95 kJ mol^{-1}) follows, corresponding to H-bonded pyridine.

From the initial slopes of the plots of integral heat of adsorption versus coverage, initial differential heats of pyridine adsorption can be determined to be 219 and 214 kJ

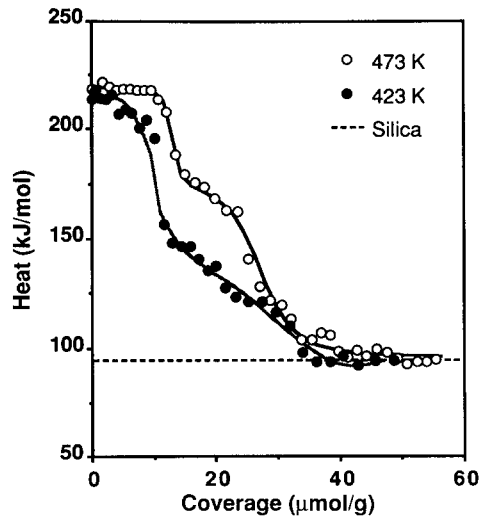

FIG. 8. Differential heat of adsorption for pyridine adsorbed on Al_2O_3/SiO_2 at 423 K and 473 K and on SiO_2 at 473 K after oxidation at 723 K (○, 473 K; ●, 423 K; ---, SiO_2 fit).

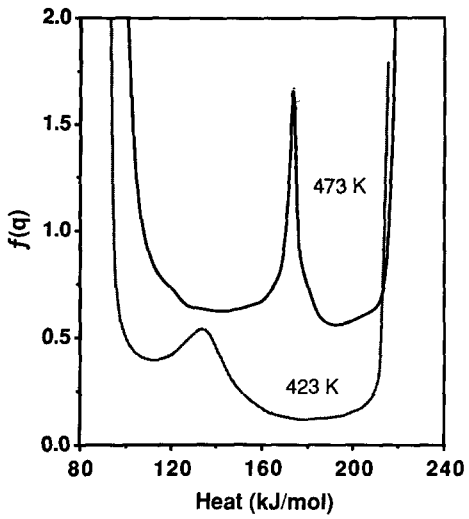

FIG. 9. Pyridine acid strength distribution for Al_2O_3/SiO_2 at 423 K and 473 K after oxidation at 723 K. The curve for adsorption at 473 K is displaced by 0.5 (μmol g^{-1})/(kJ mol^{-1}) for clarity.

mol^{-1} on Al_2O_3/SiO_2 at 473 and 423 K, respectively. Adsorption at 473 K yields a sharp step near 170 kJ mol^{-1} while the differential heat for adsorption at 423 K decreases faster and monotonously. The same conclusion can be drawn by comparing the acid strength distribution plots shown in Fig. 9. The step seen at 473 K appears as a sharp peak at 174 kJ mol^{-1} in the site strength distribution curve, while there is a broad peak with a maximum at 134 kJ mol^{-1} for adsorption at 423 K.

Additional evidence of the effect of the adsorption temperature can be obtained from plots of the thermokinetic parameter as a function of surface coverage, shown in Fig. 10. The thermokinetics of adsorption at 423 K were significantly slower than those at 473 K. All of the above data indicate that adsorption at 473 K is more specific than that at 423 K and this result agrees with results of pyridine and ammonia adsorption on H–Y zeolites and ammonia adsorption on silica–alumina at 313–473 K (*34*). Higher temperatures were not studied here because of experimental difficulties, but the fact that the initial differential heat at 423 K was only slightly lower than that at 473 K suggests that we may be close to the optimum temperature for calorimetry studies.

Plots of the thermokinetic parameter versus coverage give additional information that can aid in the differentiation of strong and weak adsorption. Adsorption on Al_2O_3/SiO_2 at 473 K was initially fast and became slower as the coverage was increased, reaching a minimum rate before a significant acceleration of the process was observed upon approaching high coverages. The adsorption rate is initially fast because the pyridine molecules are bonded irreversibly to the strongest acid sites. The adsorption rate decreases at intermediate coverages because a smaller number of strong sites are available and the molecules must diffuse over greater distances on the surface. The minimum rate appears as a maximum in the plot of the thermokinetic parameter at a coverage of about 19 μmol g^{-1}, which corresponds to a differential heat of 172 kJ mol^{-1}. Indeed, this coverage corresponds to the filling of the acid sites of intermediate strength. As the coverage is in-

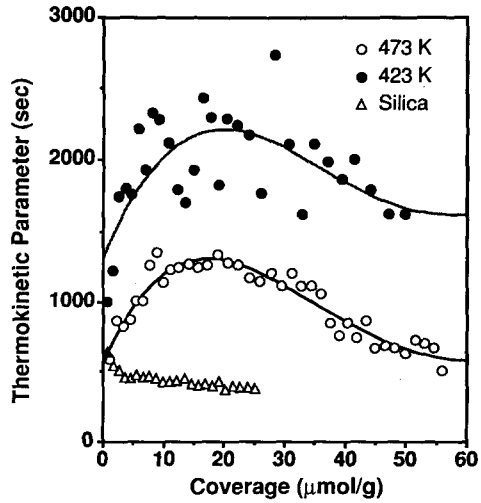

FIG. 10. Thermokinetic parameter for pyridine adsorption on Al_2O_3/SiO_2 at 423 K and 473 K and on SiO_2 after oxidation at 723 K (○, 473 K; ●, 423 K; △, SiO_2).

creased, adsorption on the support starts to dominate and the thermokinetic parameter decreases to the value for silica.

The curve for the differential heat of adsorption at 473 K displays three definite steps. This behavior apparently corresponds to the presence of several types of centers on the surface with different heat of adsorption. The possibility of surfaces with discrete inhomogeneity was suggested first by Langmuir (*45*). Klyachko (*46*) used Langmuir's model to propose an equation that describes the dependence of the differential heat of adsorption on the amount adsorbed on a surface with discrete sites. Accordingly, for s sites on the surface, the coverage will be

$$\theta = \sum_{i=1}^{s} \theta_i = \sum_{i=1}^{s} \frac{\chi_i K_i p}{1 + K_i p} = \sum_{i=1}^{s} \frac{n_i}{n_m}, \quad (5)$$

where χ_i is the fraction of centers i and n_i and n_m are the amounts adsorbed on site i (i.e., μmol g^{-1} or μmol m^{-2}) and the maximum adsorption capacity, respectively. For large differences among the equilibrium constants the different types of sites are filled successively. At equilibrium, the amount adsorbed, n, is distributed among all types of sites and the pressure is equal above all sections of the sample:

$$p_1 = p_i = p = \frac{n_1}{K_1(n_{1m} - n_1)} = \frac{n_i}{K_i(n_{im} - n_i)}. \quad (6)$$

A selectivity or distribution coefficient is defined as

$$\alpha_{1,i} = \frac{K_1}{K_i} = \exp\left\{\frac{\Delta S_1 - \Delta S_i}{R}\right\} \exp\left\{\frac{q_1 - q_i}{RT}\right\}, \quad (7)$$

where ΔS_i is the entropy of adsorption for site i. It then follows that

$$n_i = \frac{n_1 n_{im}}{n_{1m}\alpha_{1,i} - n_1(\alpha_{1,i} - 1)} \quad (8)$$

and

$$n = \sum_{i=1}^{s} n_i = \sum_{i=1}^{s} \frac{n_1 n_{im}}{n_{1m}\alpha_{1,i} - n_1(\alpha_{1,i} - 1)} \quad (9)$$

is the amount adsorbed as a function of n_1 (the adsorption on the first site).

In terms of the differential heat of adsorption on site i, q_i, the integral heat of adsorption, Q, is given by

$$Q = \sum_{i=1}^{s} q_i n_i = \sum_{i=1}^{s} \frac{n_1 n_{im} q_i}{n_{1m}\alpha_{1,i} - n_1(\alpha_{1,i} - 1)}. \quad (10)$$

The observed differential heat of adsorption is obtained by differentiating Q with respect to n,

$$q = \frac{dQ}{dn} = \frac{\sum_{i=1}^{s} (q_i n_1 n_{im}/\{n_{1m}\alpha_{1,i} - n_1(\alpha_{1,i} - 1)\}^2)}{\sum_{i=1}^{s} (n_1 n_{im}/\{n_{1m}\alpha_{1,i} - n_1(\alpha_{1,i} - 1)\}^2)}. \quad (11)$$

On the basis of Eqs. (9) and (10), the experimental data can be fitted to obtain values for n_{im}, q_i, and $\alpha_{1,i}$. Initial estimates for n_{im} and q_i can be determined by plotting the average differential heat for individual doses, calculated by dividing the amount of heat evolved during dose i by the amount adsorbed during that dose $\bar{q}_j = \Delta Q_j/\Delta n_j$ against the coverage and choosing values by inspection.

Accordingly, the experimental integral heat data were fitted using the Langmuir model for three sites. To obtain this fit, as well as other fits in this work, the values found for silica were assigned to the third site or allowed to vary slightly around those values. A summary of the results for adsorption on Al_2O_3/SiO_2 at 423 and 473 K is presented in Table 2. The fit of the sample at 423 K is presented as a qualitative com-

TABLE 2

Parameters for Fit of Integral Heat of Pyridine Adsorption on Al_2O_3/SiO_2 at 473 and 423 K with the Langmuir Model for Three Sites

Site i	Maximum coverage $n_{m,i}$ (μ mol g^{-1})		Differential heat q_i (kJ mol^{-1})		Entropy of adsorption ΔS_i (J mol^{-1} K^{-1})	
	473 K	423 K	473 K	423 K	473 K	423 K
1	12.7	10.9	219.9	213.3	−330	−360
2	14.8	16.8	177.1	140.9	−289	−233
3	140	140	96.0	93.6	−165	−167

parison, since the Langmuir model may not apply under these nonequilibrium conditions and the values for silica at 473 K may not correspond to site 3 at 423 K. It is interesting to note that the sum of monolayer coverage for sites 1 and 2 is the same within experimental error at the two temperatures, but the fitted maximum adsorption capacity for the weaker site is about 14% higher at 423 K. Also, the fitted differential heat for site 2 at 423 K is lower than that at 473 K. The difference between these results arises, as discussed above, because the adsorption at 473 K is more specific while adsorption at 423 K yields an average distribution which is more difficult to describe by three sites with constant heats.

Another problem with the fit at 423 K is that the calculated change in entropy due to adsorption for the strongest site is higher than the pyridine gas phase entropy at 423 K (316 J mol^{-1} K^{-1}). The corresponding entropy for adsorption at 473 K is the same as the pyridine gas phase entropy at 473 K. We must note that the experimental error in the total equilibrium pressure is the largest error of all the measurements in this work, and this could cause the entropy of adsorption at 473 K to be slightly outside of the range of realistic limits (the experimental error for this sample is approximately ±6 J mol^{-1} K^{-1}). In any case, a high entropy change upon adsorption means that adsorption on those sites is irreversible and essentially pressure independent, causing the nearly vertical slope seen in Fig. 6. The entropy of adsorption for site 2 at 473 K corresponds to a loss of 88% of the gas entropy and also corresponds to irreversible adsorption.

To verify if the results found for the differential heat of adsorption and acid strength distribution plots were model independent, the integral heat data were fitted with three fifty-order polynomials. These polynomials give fourth-order polynomials for the differential heat of adsorption on differentiation and third-order polynomials for the site strength distribution plots after a second differentiation. Good agreement between the Langmuir and polynomial models is found, as illustrated by the comparisons given in Figs. 11 and 12 showing that $q(n)$ and $f(q)$ are model independent.

Infrared spectroscopy results. In a previous study of Al_2O_3/SiO_2 (*8, 11*), infrared spectra of adsorbed pyridine indicated that pyridine adsorbed on Lewis, Brønsted, and hydrogen-bonding sites and that the strongest sites were Lewis acid sites. Since the differential heat curve for Al_2O_3/SiO_2 displays three steps and from IR spectroscopy there are three types of sites on the surface, we used IR spectroscopy after incremental adsorption of pyridine to test whether these sites fill sequentially with Lewis acid sites corresponding to the first step and Brønsted sites corresponding to the second step. The

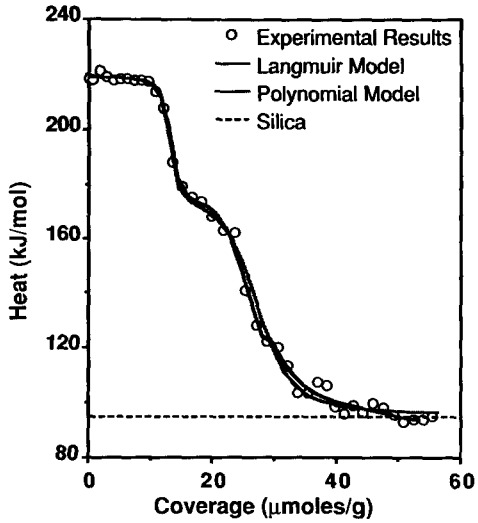

FIG. 11. Effect of the model on the determined differential heat of pyridine adsorption on Al_2O_3/SiO_2 and on SiO_2 at 473 K after oxidation at 723 K. The solid lines correspond to fits of the data with the Langmuir and polynomial models.

TABLE 3

Infrared Absorption Frequencies (cm^{-1}) for Pyridine Adsorbed on Al_2O_3/SiO_2 at 473 K as Shown in Fig. 13

Type	Band	Coverage (μmol g^{-1})				Desorption[e]
		9[a]	17[b]	22[c]	25[d]	
LPY	19b	1456.2	1456.2	1456.1	1456.0	1456.9
	19a	1496.8	1496sh	1496sh	1491.9	1496.9
	8b		1577.1	1577.0	1578.2	1579.7
	8a	1624.3	1624.1	1624.0	1624.0	1624.3
BPY	19b		1545.8	1546.8	1547.3	
	19a		1491.9	1491.9	1491.9	
	8b		1577.1	1577.0	1578.2	
	8a		1638.3	1638.3	1638.5	
HPY	19b			1446sh	1446sh	
	19a				1491.9	
	8b				1578.2	
	8a			1597.0	1596.7	

Note. sh, shoulder; LPY, pyridine bonded to a Lewis acid site; BPY, pyridine bonded to a Brønsted acid site; HPY, hydrogen-bonded pyridine.

[a] Dose 1.
[b] Dose 3.
[c] Dose 2.
[d] Dose 4.
[e] After evacuation at 673 K for 1 h.

infrared data presented in Fig. 13 and Table 3 show that after a dose of approximately 9 μmol g^{-1} bands due to Lewis sites (LPY) appear at 1624 cm^{-1} (8a) and at 1456 cm^{-1} (19b), but there is no evidence for Brønsted sites or hydrogen-bonded pyridine. After a second dose and a coverage of about 17 μmol g^{-1}, the characteristic bands for Brønsted sites appear at 1638 cm^{-1} (8a) and at 1546 cm^{-1} (19b) while there is still no evidence of hydrogen-bonded pyridine. It is not until the third dose and a coverage of 22 μmol g^{-1} that bands appear at 1597 cm^{-1} (8a) and at 1446 cm^{-1} (19b) indicating the presence of hydrogen-bonded pyridine. An additional dose at a coverage of 25 μmol g^{-1} did not show a significant increase in the intensity of the peaks for either Lewis or Brønsted sites, but the bands for hydrogen-bonded pyridine increased. Desorption at 673 K left only pyridine adsorbed on Lewis acid sites.

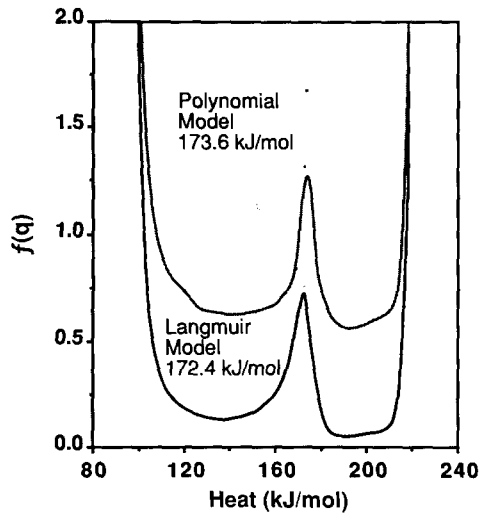

FIG. 12. Effect of the model on the determined pyridine acid strength distribution on Al_2O_3/SiO_2 at 473 K after oxidation at 723 K.

Both the incremental adsorption and the desorption IR spectra provide evidence that the strongest sites are Lewis sites. The appearance of hydrogen-bonded pyridine after the third dose is consistent with the fit of the calorimetric data. After the third dose, the calculated coverage for site 3 is about 0.7 μmol g^{-1}, whereas this coverage is about 0.001 and 0.2 μmol g^{-1} for the pre-

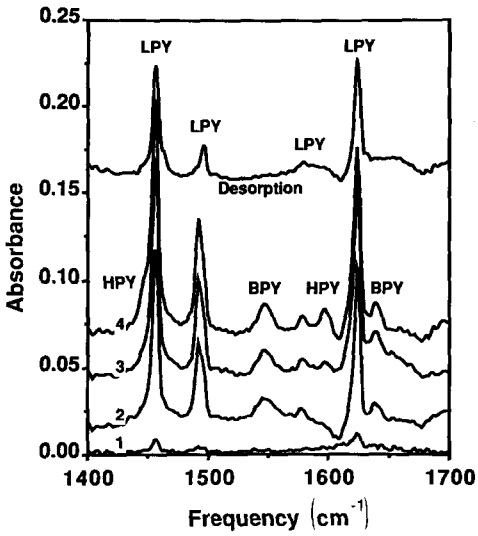

FIG. 13. Infrared spectra of pyridine adsorbed on Al_2O_3/SiO_2 at 473 K after oxidation at 723 K. Numbers 1 through 4 correspond to successive doses of pyridine and the spectrum labeled desorption was taken after desorption at 673 K for 4 hours. LPY, peak corresponding to pyridine bonded to a Lewis acid site; BPY, peak corresponding to pyridine bonded to a Brønsted acid site; and HPY, peak corresponding to hydrogen-bonded pyridine.

vious doses, which is below the detection limit of the instrument. Therefore, the assignment of silica to site 3 is justified. The results for site 2 are not conclusive, though, because the intensities of both Lewis and Brønsted bands increase after the second dose. This means either that there are weaker Lewis sites with differential heats of adsorption of similar magnitude to those of the Brønsted sites or that our IR experimental procedure does not have enough resolution to differentiate the Brønsted acid sites alone.

Paukshtis *et al.* (*47*) determined the equilibrium constant for pyridinium ion formation on HNaY zeolite from the temperature and pyridine vapor pressure dependence of the intensity of the —OH groups IR band. With this result they estimated a heat of protonation on HNaY zeolite of 172 ± 16 kJ mol^{-1}, which agrees well with our fitted differential heat for site 2. This is additional evidence supporting our hypothesis that site 2 corresponds to Brønsted acidity. This view must be verified, however, in future experimental work.

Discussion of Pyridine Adsorption Results

We discussed earlier the importance of the adsorption temperature in attaining a true acid strength distribution. The results for adsorption of pyridine on silica–alumina at 423 and 473 K confirm this point. Adsorption at the lower temperature produced lower differential heats for the entire range of coverage studied, and the acid strength distribution curve showed a broad distribution of sites. The distribution on the sample studied at the higher temperature was more definite, with differential heats near three discrete values. These observations are indicative of more specific adsorption at 473 K and they agree with previous studies of pyridine and ammonia adsorption on H–Y zeolites and ammonia adsorption on silica–alumina at 313–473 K (*34*).

Surface diffusion appears to play an important role in the equilibration of pyridine on silica-supported oxides. Specifically, the presence of a support like silica, where adsorbed pyridine retains a significant fraction of its mobility at 473 K, helps in the equilibration of pyridine adsorbed on strong sites. Above we estimated the activation energy for surface diffusion of pyridine on silica at 473 K to be 20 kJ mol^{-1}. Using this activation energy and remembering that due to the low loadings used here there is a large excess of support sites available on the surface, the energetics of a hypothetical silica–alumina surface can be represented as shown in Fig. 14. For a pyridine molecule adsorbed on a ≥Si–OH site, it is energetically more favorable to diffuse to either another contiguous ≥Si–OH site or a stronger contiguous site (activation energy = 20 kJ mol^{-1}, if we assume that the activation energy is the same for these two processes) than to desorb to the gas phase (activation energy = 95 kJ mol^{-1}). If pyridine adsorbs on a site with a differential

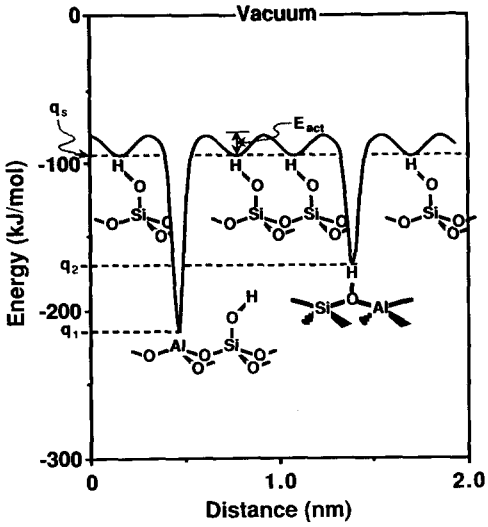

FIG. 14. Energetics for the equilibrium of pyridine between adsorption sites on a hypothetical silica–alumina surface.

heat of adsorption of 177 or 220 kJ mol^{-1}, it is still more favorable to migrate to a ≥Si–OH site than to desorb to the gas phase. In fact, the rate of desorption to the gas phase is negligible at 473 K for these strong sites. However, the rate of migration from these strong sites to the silica surface is significant. We estimate that for sites with strengths of 177 and 220 kJ mol^{-1} the rate of migration from the strong site to silica sites is 7×10^5 and slightly over 10 transitions per site each hour, respectively. Obviously, the strongest site is at the limit of what we would consider a state approaching equilibrium. For that reason it is possible that, if there are stronger sites, these could not be distinguished under our experimental conditions. It should be noted that the term in Eq. (4) due to the activation energy for surface diffusion on silica may be neglected if surface hydroxyl groups on silica are adjacent to the strong site, and this would have the effect of increasing by 20 kJ mol^{-1} the maximum heat measurable at 473 K in an equilibrium manner by calorimetry.

The interpretation given above for adsorption of pyridine on silica–alumina suggests that pyridine adsorbed on the weaker sites (sites 2 and 3) retains a significant fraction of its mobility and is able to diffuse from site-to-site. Pyridine adsorbed on the strongest sites has little or no mobility. As the coverage increases, the strongest sites are covered preferentially and a larger fraction of the pyridine is found on sites with intermediate strength. Eventually, there would be exchange between these sites and the sites on the support at high coverage. This interpretation is supported by ^{13}C and ^{15}N NMR spectroscopy results for pyridine adsorbed on silica–alumina at 433 K at different surface coverages (*48*). In that work at low coverages, nearly all of the pyridine was found to be in a low-mobility environment, and most of it was adsorbed on Lewis acid sites. Hydrogen-bonded pyridine was the dominant species on the surface for coverages higher than 0.5 monolayer, and it displayed a large mobility. Exchange-averaged species were also observed, providing evidence that exchange between mobile, weakly held species and more strongly held species was rapid on the NMR time scale (2 ms). The IR spectroscopy results found in this work for the adsorption of incremental doses of pyridine on silica–alumina are consistent with this interpretation. At low coverages, only strongly adsorbed pyridine on Lewis sites was observed; as the coverage was increased, pyridine adsorbed on both Lewis and Brønsted sites, and finally, at high coverages, the contribution from hydrogen-bonded pyridine started to dominate.

There is extensive evidence that Lewis acidity is generally stronger than Brønsted acidity (*37, 49–51*) and this was shown in particular for our samples (*8*). Specifically, the IR spectroscopy results for incremental pyridine adsorption on silica–alumina showed only pyridine adsorbed on Lewis acid sites for the initial dose. Hence, the initial differential heat of adsorption corresponds to adsorption on Lewis acid sites. The interpretation of the heats of adsorption for site 2 is not as clear as that for site

1. It is possible that site 2 corresponds to Brønsted acid sites or that it is a combination of Brønsted sites and weak Lewis sites. The IR spectroscopy results of pyridine adsorbed on silica–alumina do not provide concrete evidence to decide whether the Brønsted and weak Lewis sites have sufficiently different heat to be resolved calorimetrically.

Additional insight into the pyridine adsorption process can be obtained from the shape of the individual thermograms. The shape of these thermograms allows one to compare qualitatively the rates of the adsorption process for successive doses or for different samples via the thermokinetic parameter. The time for the heat evolution for all the doses over silica (i) was short compared to that for both the initial and the intermediate heat regions for the Al_2O_3/SiO_2 sample and (ii) comparable to that observed for the final region of low differential heat for the Al_2O_3/SiO_2 sample. The adsorption process in this latter region and over SiO_2 appears to be reversible. This agrees with the results seen by various authors (*52, 53*) and is consistent with the discussion above dealing with surface kinetics. The maximum in the thermokinetic parameter for Al_2O_3/SiO_2 was located at the end of the second step. This maximum is indicative of a change from strong to weaker adsorption, and its location is qualitatively consistent with the previous discussion of surface energetics.

The above microcalorimetric results have important implications for the measurement of acid strength using other methods. Specifically, the heat of pyridine adsorption on the silica support is quite high (95 kJ mol^{-1}), and the relative amount of pyridine adsorbed on the support, compared to that adsorbed on the stronger acid sites, may be appreciable at high pressures and low temperatures. This explains the difficulty that other investigators have had in using adsorption isotherms of basic molecules (such as pyridine) to estimate heats of adsorption by plotting ln P versus $1/T$ at constant coverage; i.e., at the pressures typically used the isotherms are dominated by contributions from the support. Our data also explain why temperature-programmed desorption of pyridine from porous catalysts generally leads to broad peaks, i.e., desorption followed by readsorption on the support takes place.

In summary, the following important conclusions result from the present study:

- Surface diffusion plays an important role for equilibration of adsorbed pyridine molecules.
- Under appropriate conditions, microcalorimetry of adsorbed pyridine provides a probe of the acid strength distribution of the catalyst.
- Doping silica with the metal oxide increases the acidity and acid strength of the catalyst.
- The acid strength distribution of Al_2O_3/SiO_2 appears to be described by adsorption on a small number of energetically homogeneous sites.

ACKNOWLEDGMENTS

We acknowledge the support of a National Science Foundation Equipment Grant that allowed us to purchase the microcalorimeter used in this work. Furthermore, we thank the Department of Energy for the partial financial support of this work (DE-FG02-84ER13183). Finally, we thank the Graduate Professional Opportunity Program and the Chevron Corporation for financial support for one of us (N.C.M.) during different stages of this work and the University of Puerto Rico–Mayagüez for providing a leave of absence to the same author.

REFERENCES

1. Gates, B. C., Katzer, J. R., and Schuit, G. C. A., "Chemistry of Catalytic Processes." McGraw–Hill, New York, 1979.
2. Benesi, H. A., and Winquist, B. H. C., *Adv. Catal.* **27,** 98 (1978).
3. Tanabe, K., *in* "Catalysis by Acids and Bases" (B. Imelik *et al.*, Eds.), p. 1. Elsevier, Amsterdam, 1985.
4. Tanabe, K., *in* "Catalysis Science and Technology" (J. R. Anderson and M. Boudart, Eds.), Vol. 2, p. 231. Springer-Verlag, New York, 1981.
5. Ai, M., *J. Catal.* **50,** 291 (1977).

6. Knözinger, H. *in* "Advances in Catalysis" (D. D. Eley, H. Pines, and P. B. Weisz, Eds.), Vol 25, p. 184, Academic Press, New York, 1976.
7. Bakshi, K. R., and Gavalas, G. R., *J. Catal.* **38,** 312 (1975).
8. Connell, G., and Dumesic, J. A., *J. Catal.* **105,** 285 (1987).
9. Connell, G., and Dumesic, J. A., *J. Catal.* **101,** 103 (1986).
10. Connell, G., and Dumesic, J. A., *J. Catal.* **102,** 216 (1986).
11. Connell, G., Ph.D. thesis, University of Wisconsin, Madison, 1985.
12. Suárez, W., Dumesic, J. A., and Hill, C. G., Jr., *J. Catal.* **94,** 408 (1985).
13. Kataoka, T., and Dumesic, J. A., *J. Catal.* **112,** 66 (1988).
14. Paukshtis, E. A., and Yurchenko, E. N., *Russ. Chem. Rev.* **52,** 242 (1983).
15. Giamello, E., Fubini, B., Lauro, P., and Bossi, A., *J. Catal.* **87,** 443 (1984).
16. Auroux, A., Sayed, M. B., and Védrine, J. C., *Thermochim. Acta* **93,** 557 (1985).
17. Fubini, B., Della Gatta, G., and Venturello, G., *J. Colloid Interface Sci.* **64,** 470 (1978).
18. Della Gatta, G., Fubini, B., and Stradella, L., *J. Chem. Soc., Faraday Trans. 2* **73,** 1040 (1977).
19. Fubini, B., Giamello, E., Della Gatta, G., and Venturello, G., *J. Chem. Soc., Faraday Trans. 1* **78,** 153 (1982).
20. Giamello, E. and Fubini, B., *J. Chem. Soc., Faraday Trans. 1* **79,** 1995 (1983).
21. Fubini, B., Bolis, V., and Giamello, E., *Thermochim. Acta* **85,** 23 (1985).
22. Pichat, P., Mathieu, M.-V., and Imelik, B., *Bull. Soc. Chim. Fr.* **8,** 2611 (1969).
23. Kline, C. H., and Turkevich, J., *J. Chem. Phys.* **12,** 300 (1944).
24. Cabot Corporation, "Cab-O-Sil® Properties and Functions," 1985.
25. Dean, J. A., "Langes's Handbook of Chemistry," 12th ed. McGraw-Hill, New York, 1979.
26. Curthoys, G., Davydov, V. Ya., Kiselev, A. V., Kiselev, S. A., and Kuznetsov, B. V., *J. Colloid Interface Sci.* **48,** 58 (1974).
27. Connell, G., unpublished results, University of Wisconsin, 1985.
28. Bak, B., Hansen-Nygaard, L., and Rastrup-Anderson, J., *J. Mol. Spectrosc.* **2,** 361 (1958).
29. Cardona-Martínez, N., Ph.D. thesis, University of Wisconsin, Madison, 1989.
30. Wells, A. F., *in* "Structural Inorganic Chemistry," 4th ed. Clarendon, Oxford, 1975.
31. Gay, I. D., and Liang, S., *J. Catal.* **44,** 306 (1976).
32. Somorjai, G. A., "Chemistry in Two Dimensions." Cornell Univ. Press, Ithaca, New York, 1981.
33. Mitani, Y., Tsutsumi, K., and Takahashi, H., *Bull. Chem. Soc. Japan* **56,** 1917 (1983).
34. Tsutsumi, K., Mitani, Y., and Takahashi, H., *Bull. Chem. Soc. Japan* **56,** 1912 (1983).
35. Kapustin, G. I., Brueva, T. R., Klyachko, A. L., and Rubinstein, A. M., *Kinet. Katal.* **22,** 1561 (1981).
36. Kapustin, G. I., Brueva, T. R., Klyachko, A. L., Rukhadze, A. D., and Rubinshtein, A. M., *Kinet. Katal.* **23,** 972 (1982).
37. Klyachko, A. L., Bankós, I., Brueva, T. R., and Kapustin, G. I., *React. Kinet. Catal. Lett.* **29**(2), 451 (1985).
38. Bankós, I., Klyachko, A. L., Brueva, T. R., and Kapustin, G. I., *React. Kinet. Catal. Lett.* **30,** 297 (1986).
39. Kusnetsov, B. V., and Derkaui, A., *Zh. Fiz. Khim.* **57,** 1314 (1983).
40. Derkaui, A., Kiselev, A. V., and Kuznetsov, B. V., *Zh. Fiz. Khim.* **59,** 159 (1985).
41. Auroux, A., Wierzchowski, P., and Gravelle, P. C., *Thermochim. Acta* **32,** 165 (1979).
42. Auroux, A., Bolis, V., Wierzchowski, P., Gravelle, P. C., and Védrine, J. C., *J. Chem. Soc., Faraday Trans. 1* **75,** 2544 (1979).
43. Auroux, A., Gravelle, P. C., Védrine, J. C., and Rekas, M., *in* "Proceedings of the Fifth International Conference on Zeolites" (L. V. Rees, Ed.), p. 433. Heyden, 1980.
44. Védrine, J. C., Auroux, A., and Coudurier, G., *in* "Catalytic Materials, Relationship between Structure and Reactivity" (T. E. Whyte *et al.*, Eds.), Amer. Chem. Soc. Symposium Series 248, p. 253, 1984.
45. Langmuir, I., *J. Amer. Chem. Soc.* **40,** 1361 (1918).
46. Klyachko, A. L., *Kinet. Katal.* **19,** 1218 (1978).
47. Paukshtis, E. A., Soltanov, R. I., and Yurchenko, E. N., *React. Kinet. Catal. Lett.* **19,** 119 (1982).
48. Maciel, G. E., Haw, J. F., Chuang, I-S., Hawkins, B. L., Early, T. A., McKay, D. R., and Petrakis, L., *J. Amer. Chem. Soc.* **105,** 5529 (1983).
49. Taniguchi, H., Masuda, T., Tsutsumi, K., and Takahashi, H., *Bull. Chem. Soc. Japan* **52,** 2195 (1979).
50. Taniguchi, H., Masuda, T., Tsutsumi, K., and Takahashi, H., *Bull. Chem. Soc. Japan* **53,** 362 (1980).
51. Kapustin, G. I., Kustov, L.M., Glonti, G. O., Brueva, T. R., Borovkov, V. Yu, Klyachko, A. L., Rubinshtein, A. M., and Kazanskii, V. B., *Kinet. Katal.* **25,** 1129 (1984).
52. Masuda, T., Taniguchi, H., Tsutsumi, K., and Takahashi, H., *Bull. Chem. Soc. Japan* **51,** 1965 (1978).
53. Masuda, T., Taniguchi, H., Tsutsumi, K., and Takahashi, H., *J. Japan Petrol. Inst.* **22,** 67 (1979).